Monthly Notices
of the
ROYAL ASTRONOMICAL SOCIETY

MNRAS **451,** 2735–2749 (2015) doi:10.1093/mnras/stv1009

A *XMM*-Newton observation of a sample of four close dwarf spheroidal galaxies

L. Manni,[1,2] A. A. Nucita,[1,2]★ F. De Paolis,[1,2] V. Testa[3] and G. Ingrosso[1,2]

[1]*Department of Mathematics and Physics* E. De Giorgi, *University of Salento, Via per Arnesano, CP 193, I-73100, Lecce, Italy*
[2]*INFN, Sez. di Lecce, Via per Arnesano, CP 193, I-73100, Lecce, Italy*
[3]*INAF, Osservatorio Astronomico di Roma, via di Frascati 33, I-00040 Monteporzio, Italy*

Accepted 2015 May 4. Received 2015 April 30; in original form 2015 February 6

ABSTRACT

We present the results of the analysis of deep archival *XMM*-Newton observations towards the dwarf spheroidal galaxies Draco, Leo I, Ursa Major II (UMa II) and Ursa Minor (UMi) in the Milky Way neighbourhood. The X-ray source population is characterized and cross-correlated with available databases to infer their nature. We also investigate if intermediate-mass black holes are hosted in the centre of these galaxies. For Draco, we detect 96 high-energy sources, two of them possibly being local stars, while no evidence for any X-ray emitting central compact object is found. Towards the Leo I and UMa II fields of view, we reveal 116 and 49 X-ray sources, respectively. None of them correlates with the putative central black holes and only one is likely associated with a UMa II local source. The study of the UMi dwarf galaxy found 54 high-energy sources and a possible association with a source at the dwarf spheroidal galaxy centre. We put an upper limit on the luminosity of the central compact object of 4.02×10^{33} erg s^{-1}. Furthermore, via the correlation with a radio source near the galactic centre, the putative black hole should have a mass of $\left(2.76^{+32.00}_{-2.54}\right) \times 10^6\,\mathrm{M}_\odot$ and be radiatively inefficient. This confirms a previous result obtained using *Chandra* data alone.

Key words: X–rays: individual: Draco dSph – Leo I dSph – UMa II dSph – UMi dSph – black hole physics.

1 INTRODUCTION

Dwarf spheroidal galaxies (dSphs) are very peculiar star systems with a mass in the range 10^3–10^7 $\mathrm{M}_\odot$ (Martin, de Jong & Rix 2008) and they are relatively poor in stars. Consequently, they are very faint and difficult to detect and study in detail. In recent decades, the interest in dSphs has rapidly grown. Indeed, until 2001, only nine Milky Way (MW) dwarf satellites (at a distance between 16 and 250 kpc) were known (Odenkirchen et al. 2001). Recently, McConnachie (2012) listed over 100 nearby galaxies in and around the Local Group, along with their relevant physical properties.

If dSphs orbit close enough to the Galactic Centre, they may lose mass and be disrupted by the tidal forces due to the Galactic potential. Tidal effects can be easily seen in the Sagittarius dSph, which has a peculiar shape characterized by stellar debris along its orbit (see Mateo, Olszewski & Morrison 1998; Ibata et al. 2001). Tidal extension signatures for Carina and Ursa Minor dSphs were also detected by Majewski et al. (2000) and Martinez-Delgado et al. (2001). In contrast, Odenkirchen et al. (2001) showed that there is no evidence for the existence of a tail-like extension of the Draco dSph star population beyond its tidal radius.

dSphs are characterized by large mass-to-light ratios. This leads scientists to infer that they are dark matter (DM) dominated objects (see, e.g., Mateo 1997). Breddels & Helmi (2013) compared different dSph formation scenarios using a sample of DM profiles and argued that no particular model is significantly preferred. Moreover, some authors suggest different dSph growth processes, without contemplating DM content. In this respect, Yang et al. (2014), using numerical simulations, claim that a merger in M31 that occurred 8.5 Gyr ago could have ejected a tidal-tail towards our direction. So that dSphs could be generated from the interaction between the low-mass tidal dwarf galaxies and our MW.

Regarding the origin and evolution of dSphs, either they are remnants of bigger systems that are disrupted by tidal forces or affected by supernova winds, which take out the overwhelming majority of gas (Silk, Wyse & Shields 1987), or they have always been small mass systems. In the latter case, they could be the building blocks of large galaxies (with mass in the range 10^9–10^{11} $\mathrm{M}_\odot$), or, in the absence of interaction (merging or disruption), they can survive until now. To address these issues, dSphs are nowadays intensively

★E-mail: nucita@le.infn.it

studied by numerical simulations to infer their formation and evolution (Assmann et al. 2013a, 2013b; Casas et al. 2012).

Additionally, as globular clusters, dSphs host old stellar populations and, consequently, any X-ray sources are expected to be most likely low-mass X-ray binaries (LMXBs) or cataclysmic variables (CVs). However, one fundamental difference between globular clusters and dSphs is that the central stellar density can be at least two orders of magnitude smaller in dSphs (Harris 1996; McConnachie 2012). Then, at variance with globular clusters where it is thought that the high stellar density forms a nursery for LMXBs through capture, for dSphs any X-ray binary should be primordial. However, due to the old stellar population, LMXBs would turn off in a few hundred million years, making finding these systems in dSphs unlikely.

The lower stellar density of dSphs offers a contrasting environment with respect to that in globular clusters and a comparison of the X-ray source populations in the two cases may help in testing the LMXB formation scenario. This is exactly the case for the Sculptor dSph, which was studied by Maccarone et al. (2005b), who found five X-ray sources [likely X-ray binaries with a neutron star or a black hole (BH) primary] with $L_X \geq 6 \times 10^{33}$ erg s^{-1} associated with the galaxy. This discovery, from one side proves that LMXBs can exist in an old stellar environment with low stellar encounters. From the other side, it is clearly challenging for the LMXB formation theory.

Hence, one of the goals of this paper is to attempt a classification of the X-ray sources identified towards our dSph sample and pinpoint local (or candidate local) sources. Detecting X-ray sources in dSphS can, moreover, help in the investigation of the DM component in these objects. Indeed, when neutron stars form in Type II supernova explosions they get large kick velocities ($\sim$100 km s^{-1}, Podsiadlowski et al. 2004) exceeding the local escape velocity (a few km s^{-1}) due to the stellar component of the dSph. However, if dSphs have a DM halo, LMXBs (and even isolated millisecond pulsars, which are direct descendants of LMXBs) can be retained within the galaxy (Dehnen & King 2006).

DSphs are also the best candidates to host intermediate-mass black holes (IMBHs) in their gravitational cores. This clue is from extrapolating the fundamental $M_{\rm BH}$–$M_{\rm Bulge}$ relation (see, e.g., Magorrian, Tremaine & Richstone 1998, for the super massive BH case) down to typical dSph masses. In particular, IMBH masses can be evaluated either via dynamical considerations or using the Fundamental Plane relation at radio and X-ray wavelengths (see, e.g., Reines, Greene & Geha 2013; Nucita et al. 2013a, 2013b). We also mention that, within the galaxy hierarchy scenario, IMBHs may be the ground seeds for the formation of super massive BHs hosted in the centre of galaxies.

Searches for IMBHs in dSphs have been attempted recently. In a very interesting paper, Lemons et al. (2015) analysed a sample of $\sim$44 000 dSph galaxies detected by the Sloan Digital Sky Survey (SDSS) with red shift $z \leq 0.055$ and stellar mass content $M_\star \leq 3 \times 10^9$ M$_\odot$. By cross-correlating with the *Chandra* Source Catalogue, it was found that 19 galaxies have at least a detectable hard X-ray source within three half light radii. Moreover, for about half of this sample, there is the evidence that the X-ray source (possibly a massive BH candidate) is associated with the optical nucleus of the dSph. Of course, as pointed out by the authors, follow-up observations are necessary to disentangle between stellar-mass X-ray binaries and active galactic nuclei (AGNs) with an accreting BH as central engine.

On the basis of these results, we also searched the selected dSphs for X-ray sources with the typical signatures of accreting IMBHs. Although the amount of data is low, it is interesting that we find that the fraction of the galaxies in our sample that appear to host a central X-ray source is similar to that observed by Lemons et al. (2015). Also in our case, only dedicated follow-up observations may unveil the nature of the source.

The paper is structured as follows: in Section 2 we briefly describe the sample of objects used in our study. Section 3 presents the procedure used to analyse the *XMM*-Newton data. The results for the high-energy study of dSphs are reported in Section 4 and, finally, in Section 5 we address our conclusions.

2 DSPH SAMPLE

Our study is a high-energy characterization of dSphs. We select the dSph sample for which *XMM*-Newton archival data are available. We did not consider the Fornax dSph galaxy since it has already been studied in detail by Orio et al. (2010) and Nucita et al. (2013a). Here, recall that these authors found an X-ray source possibly associated with a variable star belonging to the galaxy and two more sources at the boundaries of the Fornax globular clusters GC 3 and GC 4. Furthermore, following Jardel & Gebhardt (2012), who predicted the existence of a central IMBH with mass $\sim 3 \times 10^4$ M$_\odot$, Nucita et al. (2013a) also searched for X-ray targets in the galaxy centre. For one of the possible gravitational centres reported in Stetson, Hesser & Smecker-Hane (1998), the authors found a close X-ray source. The source unabsorbed 0.2–12 keV flux is 3×10^{-15} erg s^{-1} cm^{-2} corresponding to an intrinsic luminosity of $L_X \simeq 7 \times 10^{33}$ erg s^{-1} (assuming a galaxy distance of 138 kpc): in the IMBH hypothesis (and assuming Bondi spherical accretion or in the context of a Keplerian thin disk model), the compact object seems to accrete very inefficiently.

In this paper, we focus on four galaxies[1]: Draco, Leo I, Ursa Major II (UMa II) and Ursa Minor (UMi).

2.1 Draco

The Draco dSph (at J2000 coordinates RA = $17^{\rm h}20^{\rm m}12\overset{\rm s}{.}4$ and Dec = $57^\circ54'55''$) is a MW companion galaxy. Since its discovery (Wilson 1955), this galaxy has been the target of many observational campaigns. Baade & Swope (1961) first derived the distance to the galaxy as about 99 kpc through the identification of variable stars. In addition, Draco variables were studied by Zinn & Searle (1976), Nemec (1985), Goranskij (1982), Kinemuchi et al. (2002) and Bonanos et al. (2004). More recently, Kinemuchi et al. (2008) presented a survey with the photometry of different kinds of source [270 RR Lyrae stars, nine anomalous Cepheids, two eclipsing binaries, 12 slow irregular red variables, 30 background quasi-stellar objects (QSOs) and 26 probable double-mode RR Lyrae stars]. Other photometric studies were performed by Bellazzini et al. (2002) and Rave et al. (2003).

Draco seems to host a single stellar population older than $\sim$10 Gyr (Grillmair et al. 1998; Dall'Ora et al. 2003). According to Bonanos et al. (2004), the Draco luminosity ($\sim 2 \times 10^5$ L$_\odot$) is comparable to that of the faintest luminous systems.

[1] The *XMM*-Newton observations analysed in this work (see text for details) have been already used for different purposes. As an example, Malyshev, Neronov & Eckert (2014) searched for a 3.55 keV line as the signature of DM decays (in the form of sterile neutrinos). Their analysis showed no evidence for the presence of this line in the stacked spectra of the investigated dSphs.

From NED[2] we get not only the galactic coordinates but also other interesting quantities such as the mean distance of about 82 kpc and the physical major and minor axes of 1.19 and 0.72 kpc, respectively. McConnachie (2012) reports a position angle of 89°. For our study,[3] we used five *XMM*-Newton observations (IDs 0603190101, 0603190201, 0603190301, 0603190401 and 0603190501) made in August 2009 for a total exposure time of about 90 ks.

2.2 Leo I

For Leo I (at J2000 coordinates RA = $10^h08^m28^s.1$ and Dec = 12°18′23″), NED gives a mean distance of ∼246 kpc (thus it is one of the furthest MW companions), a positional angle of 80°, and physical major and minor axes of 0.86 and 0.64 kpc, respectively. Harrington & Wilson (1950) analysed this gas-poor galaxy whose type II star population and elliptical shape suggested a similarity with the Sculptor system. The large distance from the MW and the high radial velocity, confirmed by Koch et al. (2007), suggest that Leo I is an isolated dSph, not currently affected by Galactic tidal forces. However, the presence of stars beyond the object tidal radius confirms the hypothesis that some dSphs may be perturbed at least in their outermost regions by the existence of a huge amount of DM at large distances.

Smecker-Hane et al. (2009) re-analysed the star population of this dwarf galaxy and determined the galaxy's star formation rate as a function of time. In particular, they found that Leo I has a stellar population older than previously believed and older than that of the irregular Leo A galaxy, although both systems have continuously formed stars. The evidence of a radial age gradient in the red giant branch stellar population was shown by Gullieuszik et al. (2009), who estimated the stellar ages, while Menzies et al. (2010) analysed the asymptotic giant branch variables.

In our work, we use the *XMM*-Newton observation (ID 0555870201) of about 90 ks made on 2008 November 24, the same being previously analysed by Orio et al. (2010). These authors cross-correlated their sample of X-ray detected sources with the catalogue of carbon-rich asymptotic giant branch stars in Leo I (Held et al. 2010), finding no association. As claimed by Orio et al. (2010), a few X-ray sources correlate in position with red giant branch stars (most symbiotic binary systems have red giant companions). This is consistent with our results (see Section 3).

2.3 Ursa Major II

UMa II dSph (with J2000 coordinates RA = $08^h51^m30^s$ and Dec = 63°07′48″) was discovered by Zucker et al. (2006) by analysing SDSS data. They noted its irregular and distorted shape, probably due to tidal disruption. Evidence supporting this scenario is found in morphological studies by Fellhauer et al. (2007) and Muñoz, Geha & Willman (2010), to which we refer for more detail. In spite of the dominant DM contribution scenario, Smith et al. (2013) demonstrated, via *N*-body simulations, that the observed properties can be well reproduced, in the absence of DM, by tidal mass loss. So the presence or absence of DM in UMa II is not yet a settled issue.

Another still open point is related to the star population of this dwarf galaxy. Dall'Ora et al. (2012) revealed hints, although not statistically significant, of two distinct stellar populations, with different ages and metallicities. They also detected a RR Lyrae star in UMa II and evaluated a distance of about 34.7 kpc. We use a distance of 34 kpc, as reported by NED, in the analysis of *XMM*-Newton data (ID 0650180201) obtained on 2011 April 21 with an exposure time of about 34 ks. As reported in McConnachie (2012), the galaxy half light radius is $r_h \simeq 0.15$ kpc and it has a position angle of 98°.

2.4 Ursa Minor

The fourth target of our sample is UMi dSph at J2000 coordinates RA = $15^h09^m10^s.2$ and Dec = 67°12′52″ (Falco et al. 1999).

This dSph was one of the first MW companions revealed in the past century (Wilson 1955). Walker, Mateo & Olszewski (2007) analysed the stellar velocity dispersion profiles of some dSphs, among which was UMi, observing that these remain approximately constant with the galactocentre distance. The authors also noted that the observed profiles were well fitted by models of luminous star systems immersed in a DM halo.

Regarding the star formation history, UMi has a predominantly old stellar population (with an age of about 10 Gyr) (Carrera et al. 2002). In that work, the authors studied also the stellar metallicity and claimed there was no metallicity radial gradient throughout the galaxy. According to NED, UMi has a mean distance of 73 kpc, a positional angle of 69°, and physical major and minor axes of 0.85 and 0.53 kpc, respectively.

We analysed two *XMM*-Newton observations (ID 0301690301 and 0301690401) made between the end of August and the beginning of September 2005 for a total exposure time of ∼27 ks.

Nucita et al. (2013b) analysed the X-ray data acquired by the *Chandra* satellite towards this galaxy and found an X-ray source spatially coincident with a radio one (within a few arcseconds). Assuming that the target is an accreting IMBH, the authors evaluated the BH mass to be $\sim 2.9 \times 10^6$ $M_\odot$. However, the detection algorithm used did not allow us to exclude that one false detection per CCD may have occurred. To confirm the previous result, here we used *XMM*-Newton observations (see the next section).

3 *XMM*-NEWTON DATA REDUCTION AND SOURCE DETECTION

We used the XMM-SCIENCE ANALYSIS SYSTEM (SAS)[4] with the most recent calibration files to process the observation data files (ODFs).

We obtained the event lists by processing the raw data via the standard EMCHAIN and EPCHAIN tools, and following the standard procedures in screening the data provided by the three European Photon Imaging Camera (EPIC) systems, MOS 1, MOS 2 and pn, on board the *XMM*-Newton satellite.

[2] The NASA/IPAC Extragalactic Database is available at http://ned.ipac.caltech.edu.

[3] For completeness, we note that Draco dSph was observed also by the *Chandra* satellite (IDs 9568 and 9776) with the ACIS-S camera and exposure times of ∼24 and ∼12 ks, respectively. Only four detectors were on during the observations, thus limiting the coverage of the Draco galaxy. The event files were reprocessed using the most up-to-date calibration files and the CIAO tool suite (version 4.6). Then, we searched for X-ray sources in 0.5–7 keV using the CELLDETECT code, choosing a signal-to-noise ratio of 2.5 for source detection. After eliminating a few sources not recognized as such by eye, we were left with nine X-ray targets indicated by yellow diamonds in Fig. 1. Recall that the background corrected rates and fluxes of the identified sources are consistent within the errors with those estimated using *XMM*-Newton.

[4] http://xmm.esa.int/sas/

We applied the analysis procedure described in Nucita et al. (2013a). Here, recall that, in accordance with the 2XMM catalogue of serendipitous X-ray sources (Watson et al. 2009), we divided each EPIC camera event list into five energy bands (B_1: 0.2–0.5 keV, B_2: 0.5–1.0 keV, B_3: 1.0–2.0 keV, B_4: 2.0–4.5 keV and B_5: 4.5–12.0 keV), producing one image for each energy band, plus a mosaic image in the 0.2–12.0 keV energy band (for inspection only), and detected the sources using the SAS task EDETECT_CHAIN.

The exposure map was evaluated with the EEXPMAP task, for each camera and input image, taking into account the calibration information on spatial quantum efficiency, filter transmission and vignetting. Then, we produced appropriate image masks to delimit the regions for source detection with the task EMLDETECT. This task applies a point spread function fitting algorithm simultaneously in the five energy bands giving as output source coordinates, energy fluxes and hardness ratios (HRs); for details, see: http://xmm.esac.esa.int/sas/current/documentation.

The X-ray fluxes are given in units of erg s^{-1} cm^{-2} through

$$F_i = \frac{B_i}{\mathrm{ECF}_i}, \quad (1)$$

where the count rate (B_i) and the energy conversion factor (ECF$_i$) are in units of 10^{11} counts cm^2 erg^{-1} in the ith band for each EPIC camera. To obtain the latter factors we assumed a power-law model with photon index $\Gamma = 1.7$ and mean Galactic foreground absorption $N_{\rm H} \simeq 3.0 \times 10^{20}$ cm^{-2} (Watson et al. 2009).[5]

Finally, we purged the candidate source lists by requiring a maximum likelihood threshold equal to 10, corresponding to 4σ, and removing a few spurious sources identified as false detections or positioned at the borders of the cameras. Our results are consistent with the 3XMMi-DR4 data with minor differences because of the exclusion of the spurious sources.

At the end of the procedure, we obtained 89, 116, 49 and 54 sources for Draco, Leo I, UMa II and UMi, respectively. Previously, Orio et al. (2010) analysed the same Leo I data set detecting 105 X-ray sources. We impute the discrepancy to slightly different choices in the data screening procedure and the detection threshold used.

The logarithmically scaled 0.2–12 keV images (smoothed with a 3 pixel Gaussian kernel) are shown in Fig. 1. For Draco, Leo I and UMi, the dashed ellipses represent the extension of the galaxies as suggested by NED, while for UMa II we used the half light radius taken from McConnachie (2012). In each panel, the 35 arcsec radius circles containing ∼90 per cent of energy at 1.5 keV as measured by the pn camera (see, e.g., de la Calle et al. 2008) indicate the detected sources, each of which is labelled with a sequential number following the 0.2–12.0 keV increasing flux order.

In Tables 1–4 we report the main results of our analysis, showing the detected sources in increasing flux order. For each source, the first two columns show, respectively an identification number and a label (#) indicating how many times it was revealed in the *XMM*-Newton observations: A, once; B, twice; C, three times, and so on. For Leo I and UMa II, there are only A sources because we used a single observation. Columns 3–5 report the J2000 coordinates with the associated errors. Column 6 reports the 0.2–12.0 keV absorbed flux. To get the parameter $\log(f_X/f_{\rm opt})$ (column 7), the SIMBAD[6] archive was searched for correlations (within a radius of 3 arcsec) from which we extracted the relevant magnitude in the V band or, if not available, the average of the R and B bands (Bartlett et al. 2012). The high-energy hardness ratios HR_1^*, HR_2^* and HR_i with $i = 1, \ldots, 4$ (see next section) are shown in the remaining columns.

In Tables 5–8 we present the correlation with catalogued counterparts, if any. For this purpose, we used several databases to correlate our X-ray source catalogue with optical counterparts, namely: the Two Micron All-Sky Survey (2MASS), the Two

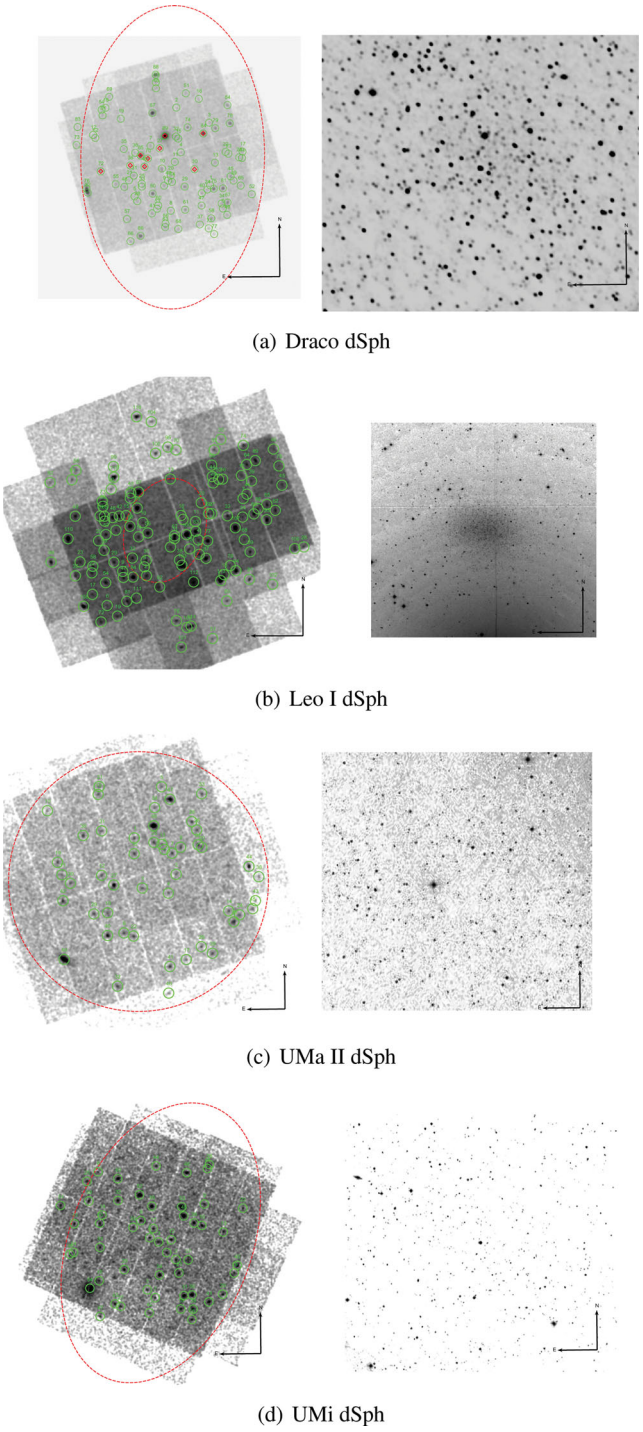

(a) Draco dSph

(b) Leo I dSph

(c) UMa II dSph

(d) UMi dSph

Figure 1. Mosaic images of the *XMM*-Newton, MOS 1, MOS 2 and pn exposures in the 0.2–12.0 keV energy band for the sample galaxies.

[5] For ECFs and associated correction factors, see the User's Guide of the 2XMM catalogue of serendipitous sources available at http://xmmssc-www.star.le.ac.uk/Catalogue/2XMMi-DR3. Note that our results are consistent within a few per cent when relaxing the adopted assumptions.

[6] http://simbad.u-strasbg.fr/simbad/

Table 1. X-ray sources towards the Draco dSph as detected by the *XMM*-Newton satellite. The full list is available online.

Source	#	RA (J2000)	Dec (J2000)	Err (arcsec)	$F^{\rm Abs}_{0.2-12\,\rm keV}$ $\times 10^{-14}$ erg s^{-1} cm^{-2}	$\log\left(\frac{f_X}{f_{\rm opt}}\right)$	$\rm HR_1^*$	$\rm HR_2^*$	$\rm HR_1$	$\rm HR_2$	$\rm HR_3$	$\rm HR_4$
1	A	17 19 26.1	57 50 18.7	2.546	$\leq$1.21	–	0.08 ± 0.58	−0.66 ± 0.67	0.71 ± 0.22	−0.83 ± 0.20	−1.00 ± 1.01	1.00 ± 0.64
2	A	17 20 07.8	58 03 5.8	2.558	$\leq$1.09	0.131	−0.07 ± 0.64	−0.26 ± 0.68	0.01 ± 0.30	0.29 ± 0.30	−1.00 ± 0.22	1.00 ± 0.23
3	A	17 19 27.2	58 00 36.3	2.418	0.54 ± 0.45	−1.314	0.28 ± 0.55	−0.44 ± 0.56	−0.11 ± 0.29	−0.35 ± 0.29	−0.76 ± 0.47	1.00 ± 0.14
4	C	17 20 02.3	57 55 44.5	2.510	0.55 ± 0.27	–	−0.08 ± 0.63	−0.13 ± 0.69	0.18 ± 0.25	0.01 ± 0.25	−0.24 ± 0.31	−0.64 ± 0.37
5	A	17 20 59.4	57 48 28.7	2.567	$\leq$1.29	–	−0.22 ± 0.73	−0.09 ± 0.64	−0.04 ± 0.20	0.27 ± 0.24	−0.46 ± 0.27	−0.94 ± 0.94
6	A	17 19 10.6	57 46 28.3	2.591	$\leq$1.31	–	−0.13 ± 0.79	−0.02 ± 0.59	0.37 ± 0.31	0.28 ± 0.25	−0.42 ± 0.26	−1.00 ± 0.93
7	A	17 20 39.8	57 56 48.2	2.427	0.66 ± 0.37	–	0.09 ± 0.65	0.23 ± 0.56	−0.10 ± 0.31	0.68 ± 0.21	−0.13 ± 0.25	−0.23 ± 0.31
8	A	17 20 14.7	57 46 07.5	2.578	0.70 ± 0.62	–	−0.14 ± 0.68	0.14 ± 0.59	0.35 ± 0.31	0.28 ± 0.22	−0.20 ± 0.23	−1.00 ± 0.48
9	B	17 20 22.9	57 50 14.8	3.287	0.71 ± 0.33	–	0.00 ± 0.63	0.20 ± 0.57	0.67 ± 0.44	0.53 ± 0.23	0.01 ± 0.21	−0.75 ± 0.21

Table 2. X-ray sources towards the Leo I dSph as detected by the *XMM*-Newton satellite. The full list is available online.

Source	#	RA (J2000)	Dec (J2000)	Err (arcsec)	$F^{\rm Abs}_{0.2-12\,\rm keV}$ $\times 10^{-14}$ erg s^{-1} cm^{-2}	$\log\left(\frac{f_X}{f_{\rm opt}}\right)$	$\rm HR_1^*$	$\rm HR_2^*$	$\rm HR_1$	$\rm HR_2$	$\rm HR_3$	$\rm HR_4$
1	A	10 08 56.2	12 19 27.2	2.480	0.15 ± 0.14	–	−0.16 ± 0.60	−0.01 ± 0.49	0.27 ± 0.26	0.09 ± 0.22	−0.76 ± 0.24	0.42 ± 0.38
2	A	10 08 50.9	12 18 24.8	2.403	0.20 ± 0.15	–	−0.39 ± 0.54	−0.03 ± 0.49	0.20 ± 0.22	0.22 ± 0.17	−0.95 ± 0.14	0.76 ± 1.14
3	A	10 08 19.5	12 19 38.6	2.344	0.21 ± 0.13	−0.870	−0.12 ± 0.59	−0.17 ± 0.57	−0.03 ± 0.22	−0.03 ± 0.24	−0.40 ± 0.33	0.06 ± 0.51
4	A	10 08 12.4	12 17 18.7	2.358	0.21 ± 0.14	–	−0.32 ± 0.53	0.04 ± 0.46	0.63 ± 0.17	−0.08 ± 0.16	−0.35 ± 0.21	−0.99 ± 0.71
5	A	10 08 25.4	12 16 29.9	2.358	0.22 ± 0.11	–	−0.15 ± 0.37	−0.53 ± 0.46	0.27 ± 0.16	−0.44 ± 0.18	−0.86 ± 0.35	0.34 ± 0.85
6	A	10 08 55.0	12 09 47.9	2.475	$\leq$0.50	–	−0.06 ± 0.77	−0.52 ± 0.77	−0.22 ± 0.20	−0.19 ± 0.26	−0.22 ± 0.40	−1.00 ± 1.39
7	A	10 07 51.4	12 22 01.9	2.408	$\leq$0.58	–	0.08 ± 0.77	0.02 ± 0.54	−0.98 ± 0.12	0.98 ± 0.16	−0.20 ± 0.30	0.09 ± 0.34
8	A	10 08 37.6	12 14 13.2	2.350	0.26 ± 0.17	–	−0.18 ± 0.52	−0.05 ± 0.45	0.26 ± 0.22	0.11 ± 0.20	−0.47 ± 0.24	0.33 ± 0.51
9	A	10 08 47.8	12 13 41.6	2.651	0.30 ± 0.12	–	−0.14 ± 0.38	−0.08 ± 0.36	0.49 ± 0.18	0.06 ± 0.15	−0.28 ± 0.18	−0.99 ± 0.40
10	A	10 08 38.3	12 19 17.1	2.321	0.33 ± 0.15	–	−0.21 ± 0.52	−0.12 ± 0.46	−0.09 ± 0.17	0.32 ± 0.19	−0.94 ± 0.16	0.81 ± 0.50

Table 3. X-ray sources towards the UMa II dSph as detected by the *XMM*-Newton satellite. The full list is available online.

Source	#	RA (J2000)	Dec (J2000)	Err (arcsec)	$F^{\rm Abs}_{0.2-12\,\rm keV}$ $\times 10^{-14}$ erg s^{-1} cm^{-2}	$\log\left(\frac{f_X}{f_{\rm opt}}\right)$	$\rm HR_1^*$	$\rm HR_2^*$	$\rm HR_1$	$\rm HR_2$	$\rm HR_3$	$\rm HR_4$
1	A	08 51 34.3	63 12 48.2	2.414	0.67 ± 0.48	–	−0.24 ± 0.41	−0.45 ± 0.50	0.58 ± 0.17	−0.38 ± 0.17	−0.90 ± 0.23	−1.00 ± 2.82
2	A	08 50 51.9	63 08 37.6	2.578	0.68 ± 0.25	–	−0.08 ± 0.65	0.30 ± 0.65	0.15 ± 0.42	0.64 ± 0.23	−0.16 ± 0.23	−1.00 ± 0.19
3	A	08 51 26.3	63 07 03.7	2.431	0.69 ± 0.32	–	−0.08 ± 0.52	−0.08 ± 0.55	0.56 ± 0.27	0.28 ± 0.22	−0.32 ± 0.22	−0.38 ± 0.35
4	A	08 50 59.9	63 06 28.6	2.496	0.80 ± 0.48	–	−0.23 ± 0.71	0.22 ± 0.63	0.25 ± 0.39	0.54 ± 0.24	−0.47 ± 0.22	−0.93 ± 0.49
5	A	08 51 06.5	63 18 38.9	2.708	0.83 ± 0.56	–	−0.31 ± 0.51	−0.24 ± 0.59	0.67 ± 0.19	−0.17 ± 0.22	−0.90 ± 0.15	−1.00 ± 0.73
6	A	08 51 03.7	63 11 29.1	2.449	0.87 ± 0.32	–	−0.30 ± 0.57	0.06 ± 0.56	0.53 ± 0.28	0.15 ± 0.20	−0.41 ± 0.24	−0.89 ± 0.30
7	A	08 50 55.9	63 11 02.2	2.246	1.01 ± 0.37	–	−0.21 ± 0.32	−0.44 ± 0.41	0.48 ± 0.14	−0.44 ± 0.15	−0.85 ± 0.25	−0.29 ± 0.82
8	A	08 51 44.6	63 01 55.2	2.303	1.18 ± 0.51	–	−0.29 ± 0.39	−0.19 ± 0.45	0.43 ± 0.17	−0.04 ± 0.17	−0.81 ± 0.17	0.62 ± 0.45
9	A	08 50 47.3	63 11 43.6	2.323	1.20 ± 0.50	–	−0.21 ± 0.41	−0.08 ± 0.43	0.14 ± 0.23	0.34 ± 0.16	−0.66 ± 0.16	−0.49 ± 0.46
10	A	08 53 02.7	63 15 53.0	2.505	$\leq$3.14	–	−0.10 ± 0.50	−0.46 ± 0.59	0.51 ± 0.27	−0.21 ± 0.27	−0.70 ± 0.27	−1.00 ± 0.92

Table 4. X-ray sources towards the UMi dSph as detected by the *XMM*-Newton satellite. The full list is available online.

Source	#	RA (J2000)	Dec (J2000)	Err (arcsec)	$F^{\rm Abs}_{0.2-12\,\rm keV}$ $\times 10^{-14}$ erg s^{-1} cm^{-2}	$\log\left(\frac{f_X}{f_{\rm opt}}\right)$	$\rm HR_1^*$	$\rm HR_2^*$	$\rm HR_1$	$\rm HR_2$	$\rm HR_3$	$\rm HR_4$
1	A	15 09 01.8	67 11 31.9	2.582	0.59 ± 0.34	−0.923	−0.32 ± 0.66	0.16 ± 0.70	−0.20 ± 0.35	0.38 ± 0.28	−0.38 ± 0.24	−1.00 ± 0.31
2	A	15 08 48.6	67 10 34.6	2.708	0.72 ± 0.59	–	−0.34 ± 0.79	0.20 ± 0.83	0.17 ± 0.44	0.37 ± 0.28	−0.28 ± 0.23	−0.66 ± 0.40
3	A	15 09 13.1	67 12 59.4	3.052	0.73 ± 0.29	–	−0.18 ± 0.52	−0.33 ± 0.67	0.42 ± 0.24	−0.33 ± 0.24	−0.66 ± 0.19	−1.00 ± 0.29
4	A	15 09 25.9	67 13 35.3	2.477	0.85 ± 0.45	–	−0.25 ± 0.73	0.27 ± 0.71	0.71 ± 0.23	0.37 ± 0.26	−0.51 ± 0.24	−0.17 ± 0.38
5	A	15 09 29.2	67 06 24.6	2.779	0.88 ± 0.64	−0.402	−0.19 ± 0.45	−0.23 ± 0.54	0.24 ± 0.31	−0.01 ± 0.28	−0.39 ± 0.32	−1.00 ± 1.03
6	A	15 10 39.6	67 22 36.6	2.912	$\leq$3.59	0.717	−0.01 ± 0.98	−0.49 ± 0.96	−0.01 ± 0.29	−0.32 ± 0.39	−0.09 ± 0.90	−1.00 ± 2.72
7	A	15 09 18.0	67 05 20.3	2.607	0.98 ± 0.67	–	−0.06 ± 0.33	−0.67 ± 0.45	0.51 ± 0.22	−0.74 ± 0.17	−0.29 ± 0.58	−1.00 ± 1.63
8	A	15 09 38.4	67 15 56.0	2.414	1.12 ± 0.51	0.507	−0.42 ± 0.58	0.28 ± 0.56	−0.01 ± 0.24	0.61 ± 0.15	−0.76 ± 0.18	−0.49 ± 0.47
9	A	15 08 08.1	67 18 10.8	2.573	1.17 ± 0.89	0.478	−0.14 ± 0.55	−0.39 ± 0.63	0.11 ± 0.24	−0.01 ± 0.25	−0.78 ± 0.26	0.62 ± 0.53
10	A	15 08 11.7	67 15 14.4	2.339	1.24 ± 0.82	0.407	−0.19 ± 0.47	−0.26 ± 0.49	0.13 ± 0.20	−0.04 ± 0.20	−0.36 ± 0.23	−1.00 ± 0.82

Micron All-Sky Survey Extended objects (2MASX, Skrutskie et al. 2006), the United States Naval Observatory all-sky survey (USNO-B1, Monet, Levine & Canzian 2003), the position and proper motion extended catalogues (PPMX, Roeser et al. 2008 and PPMXL, Roeser, Demleitner & Schilbach 2010), the QSO candidates in the examined SDSS stripes (J/MNRAS/396/223/qsos, D'Abrusco, Longo & Walton 2009) and the candidate AGN objects catalogue (J/MNRAS/437/968, Cavuoti et al. 2014). Regarding Draco dSph, we also searched for long-period, semi-regular red variable stars, carbon stars and eclipsing binaries (J/AJ/136/1921/table9, Kinemuchi et al. 2008), QSOs found in the same survey (J/AJ/136/1921/table10, Kinemuchi et al. 2008), variable stars (J/AJ/127/861, Bonanos et al. 2004) and late-type stars (J/A+A/442/165, Cioni & Habing 2005). The quasar–galaxy association catalogue (J/AZh/78/675, Bukhmastova 2001) was used in the analysis for both Draco and UMi.

For Leo I, we used the NIR catalogue obtained with the WFCAM wide-field array at the United Kingdom Infrared Telescope (J/MNRAS/404/1475/table2, Held et al. 2010), while the Palomar Transient Factory photometric catalogue 1.0 (II/313, Ofek et al.

Table 5. Correlation of the X-ray sources towards the Draco dSph. The full list is available online.

Source	RA (J2000)	Dec (J2000)	223/qsos (arcsec)	2MASS (arcsec)	2MASX (arcsec)	PPMX (arcsec)	PPMXL (arcsec)	USNO-B1 (arcsec)	table9 (arcsec)	table10 (arcsec)	437/968 (arcsec)	127/861 (arcsec)	78/675 (arcsec)	442/165 (arcsec)	SIMBAD O type	HR class
1	17 19 26.1	57 50 18.7	–	1.46	–	1.46	1.46	–	–	–	–	–	–	–	–	f
2	17 20 07.8	58 03 5.8	–	–	–	–	0.13	0.58	–	–	–	–	–	–	*	fg
3	17 19 27.2	58 00 36.3	–	1.86	–	–	1.82	1.65	–	–	–	–	–	–	*	FG
4	17 20 02.3	57 55 44.5	–	–	–	–	–	–	–	–	–	–	–	–	–	–
5	17 20 59.4	57 48 28.7	–	–	–	–	–	–	–	–	–	–	–	–	–	f
6	17 19 10.6	57 46 28.3	–	–	–	–	–	–	–	–	–	–	–	–	–	f
7	17 20 39.8	57 56 48.2	–	–	–	–	–	–	–	–	–	–	–	–	–	h
8	17 20 14.7	57 46 07.5	–	–	–	–	–	–	–	–	–	–	–	–	–	h
9	17 20 22.9	57 50 14.8	–	–	–	–	–	–	–	–	–	–	–	–	–	h
10	17 20 25.6	57 53 04.7	–	0.32	–	0.37	0.37	0.38	–	–	0.40	–	–	–	*	FG

Table 6. Correlation of the X-ray sources towards the Leo I dSph. The full list is available online.

Source	RA (J2000)	Dec (J2000)	223/qsos (arcsec)	2MASS (arcsec)	PPMX (arcsec)	PPMXL (arcsec)	USNO-B1 (arcsec)	437/968 (arcsec)	1475/table2 (arcsec)	SIMBAD O type	HR class
1	10 08 56.2	12 19 27.2	–	–	–	–	–	–	–	–	f
2	10 08 50.9	12 18 24.8	–	–	–	–	–	–	–	–	f
3	10 08 19.5	12 19 38.6	–	–	–	–	–	–	1.43	RG*	l
4	10 08 12.4	12 17 18.7	–	–	–	–	–	–	2.23	–	–
5	10 08 25.4	12 16 29.9	–	–	–	–	–	–	–	–	f
6	10 08 55.0	12 09 47.9	–	2.99	–	–	–	–	–	–	–
7	10 07 51.4	12 22 01.9	–	–	–	–	–	–	–	–	h
8	10 08 37.6	12 14 13.2	–	–	–	–	–	–	–	–	f
9	10 08 47.8	12 13 41.6	–	–	–	–	–	–	–	–	h
10	10 08 38.3	12 19 17.1	–	–	–	–	–	–	2.39	–	h

Table 7. Correlation of the X-ray sources towards the UMa II dSph. The full list is available online.

Source	RA (J2000)	Dec (J2000)	223/qsos (arcsec)	2MASS (arcsec)	2MASX (arcsec)	PPMX (arcsec)	PPMXL (arcsec)	USNO-B1 (arcsec)	I1/313 (arcsec)	437/968 (arcsec)	SIMBAD O type	HR class
1	08 51 34.3	63 12 48.2	–	1.86	–	–	2.63	0.77	–	–	–	f
2	08 50 51.9	63 08 37.6	–	–	–	–	–	–	–	–	–	h
3	08 51 26.3	63 07 03.7	–	–	–	–	–	–	–	–	–	h
4	08 50 59.9	63 06 28.6	–	–	–	–	–	–	–	–	–	h
5	08 51 06.5	63 18 38.9	–	–	–	–	–	–	–	–	–	f
6	08 51 03.7	63 11 29.1	–	–	–	–	–	–	–	–	–	f
7	08 50 55.9	63 11 02.2	–	0.95	–	–	0.96	0.74	0.87	–	–	f
8	08 51 44.6	63 01 55.2	–	1.27	–	–	1.33	1.77	1.31	–	–	f
9	08 50 47.3	63 11 43.6	–	–	–	–	–	–	–	–	–	h
10	08 53 02.7	63 15 53.0	–	–	–	–	–	–	–	–	–	f

Table 8. Correlation of the X-ray sources towards the UMi dSph. The full list is available online.

Source	RA (J2000)	Dec (J2000)	223/qsos (arcsec)	2MASS (arcsec)	PPMX (arcsec)	PPMXL (arcsec)	USNO-B1 (arcsec)	180/67 (arcsec)	V/134 (arcsec)	SIMBAD O type	HR class
1	15 09 01.8	67 11 31.9	–	1.10	–	0.96	0.54	–	–	*	l
2	15 08 48.6	67 10 34.6	–	–	–	–	–	–	–	–	f
3	15 09 13.1	67 12 59.4	–	–	–	–	–	–	–	–	–
4	15 09 25.9	67 13 35.3	–	–	–	–	–	–	–	–	f
5	15 09 29.2	67 06 24.6	2.28	–	–	2.22	2.41	2.29	–	*	l
6	15 10 39.6	67 22 36.6	–	–	–	–	–	–	–	*	l
7	15 09 18.0	67 05 20.3	–	–	–	–	–	–	–	–	–
8	15 09 38.4	67 15 56.0	–	–	–	–	–	–	–	*	snr
9	15 08 08.1	67 18 10.8	–	–	–	–	–	–	–	*	l
10	15 08 11.7	67 15 14.4	–	–	–	–	–	–	–	*	fg

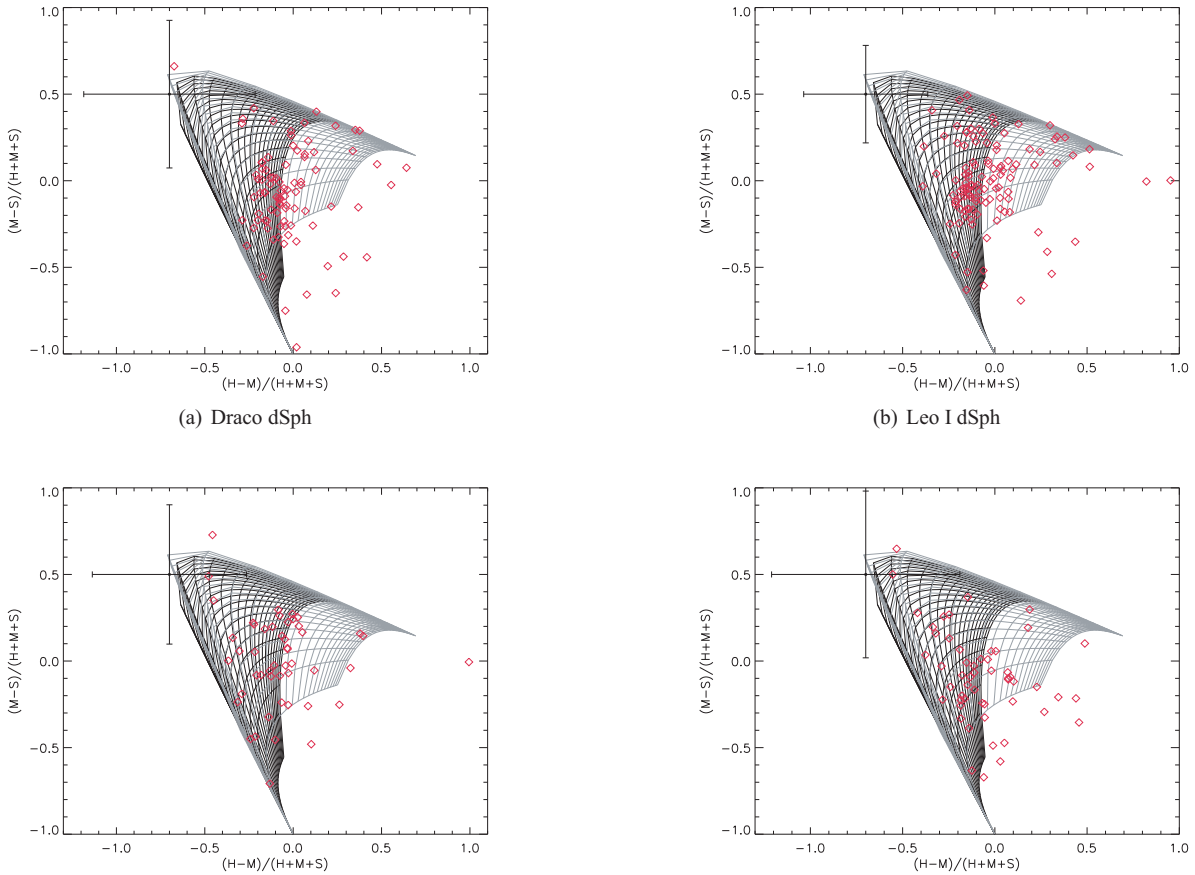

(a) Draco dSph (b) Leo I dSph

(c) UMa II dSph (d) UMi dSph

Figure 2. Colour–colour diagram of the sources detected by the EPIC cameras towards the dSphs. The solid lines represent the theoretical tracks expected for different emitting models (see text for details). A representative error bar (obtained averaging all data point error bars) is also shown in each panel.

2012) was compared with the UMa II source list. Moreover, for UMi dSph we examined the catalogue of quasar candidates from a non-parametric Bayes classifier kernel density estimate (J/ApJS/180/67, Richards et al. 2009) and the atlas of radio/X-ray associations (V/134/arxa, Flesch 2010).

For details of the limiting magnitude of the catalogues used, refer to the relevant publications. Here, for example, recall that 2MASS has limiting sensitivities of 17.1, 16.4 and 15.3 mag in the *J*, *H* and *K* bands, respectively, while the USNO-B1 catalogue is complete down to a visual magnitude of ∼21 and has positional accuracy of ∼0.2 arcsec. Note that some catalogues (PPMX and PPMXL, or 223/qsos and 437/968) refer to other well-known catalogues (such as 2MASS and USNO-B1, or SDSS) and inherit the corresponding limiting magnitudes.

Therefore, we associated the coordinates of each of the identified X-ray sources with an error resulting from the quadrature sum of the *XMM*-Newton positional accuracy (∼2 arcsec at 2σ confidence level; see Kirsch 2004 and Guainazzi 2010) and the statistical error as determined by the EDETECT_CHAIN tool. Since the resulting positional uncertainty is of the order of a few arcseconds, we do not over-plot the source error circles in any figure of this paper. In the same way, the error associated with the optical counterpart was derived from the relevant catalogues.

Only if an X-ray source is found to be within 1σ (and 3 arcsec) from a catalogue counterpart, do we report the corresponding distance in arcseconds in Tables 5–8. If there were multiple sources satisfying the previous condition, the source at the minimum distance from the X-ray target was used. We also show the object type (O type) category of the counterpart, as reported in the SIMBAD archive,[7] as well as our own source classification (HR class).

4 HIGH-ENERGY VIEW

In the following section, we address the problem of the membership of our X-ray sources to the dSph galaxies, mainly through the analysis of high-energy data.

4.1 Hardness ratios and X-ray-to-NIR flux diagrams

To attempt a classification of the high-energy sources detected towards our dSph sample, we followed Ramsay & Wu (2006) and calculated the hardness ratios (HR^*) as

$$HR_1^* = \frac{H - M}{S + M + H} \quad \text{and} \quad HR_2^* = \frac{M - S}{S + M + H}. \tag{2}$$

Here, *S*, *M* and *H* correspond to the count rates in the 0.2–1.0, 1.0–2.0 and 2.0–12.0 keV energy bands. From these HR^* values we constructed the colour–colour diagrams shown in Fig. 2, where the obtained values are compared with two spectral models.

[7] The SIMBAD object classification (class standard designation, condensed one and extended explanation as well) is available at http://simbad.u-strasbg.fr/simbad/sim-display?data = otypes.

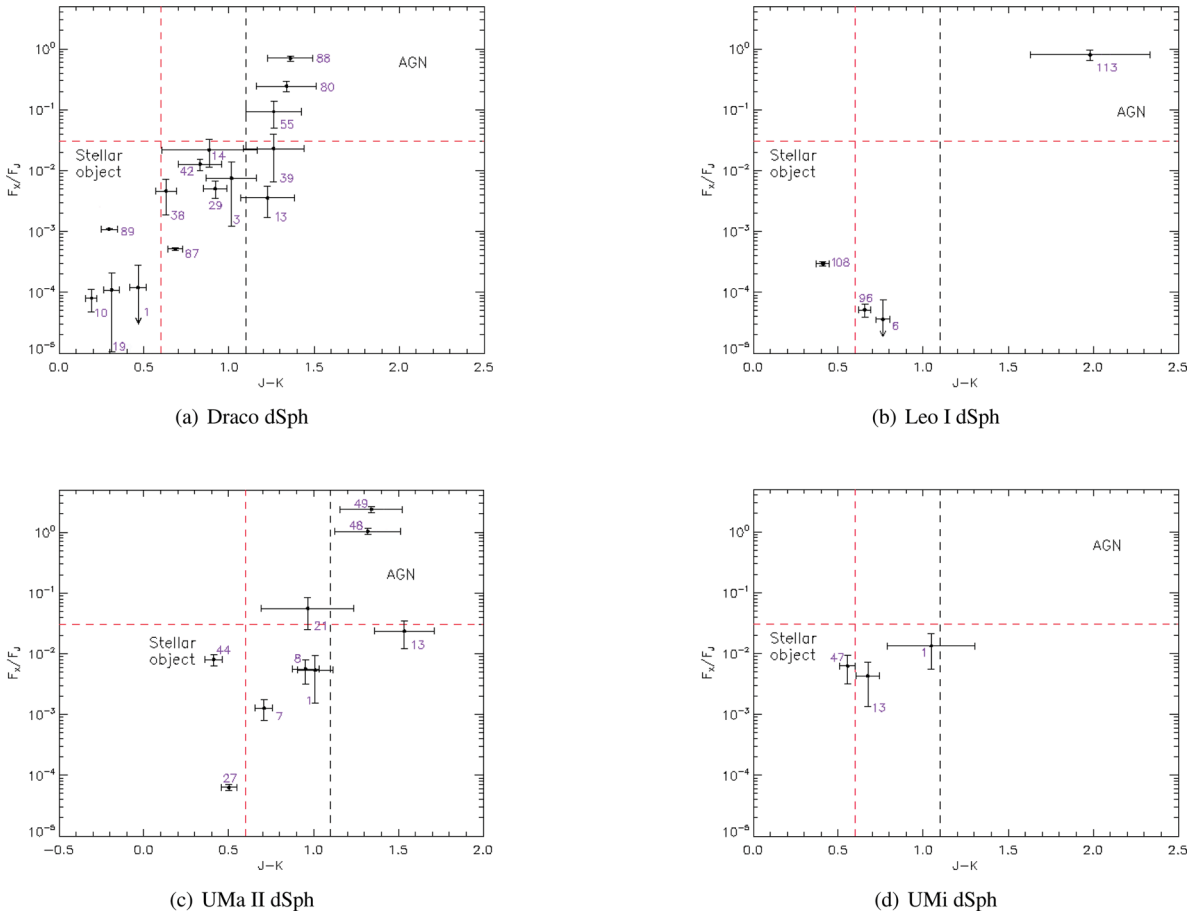

(a) Draco dSph (b) Leo I dSph

(c) UMa II dSph (d) UMi dSph

Figure 3. Colour–colour diagram for our X-ray sources with a counterpart in the 2MASS catalogue (see text for details).

We used bremsstrahlung (grey tracks) and power-law (black lines) models to simulate HR_1^* and HR_2^* of CVs, AGNs and X-ray binaries.[8]

We used the XSPEC package (Arnaud 1996) version 12.0.0 to obtain the colour–colour contours. In both cases, we vary the equivalent hydrogen column density N_H from 10^{19} to 10^{22} cm^{-2} so each of the almost horizontal lines corresponds to models with equal N_H, which increases from bottom to top. The temperature associated with each bremsstrahlung model (kT, taken in the range 0.1–3.0 keV) and the power-law index Γ (in the range 0.1–3.0) are associated with primarily vertical lines: the values of kT and Γ increase from left to right and from right to left, respectively.

In the upper left side of each panel of Fig. 2 we give a representative error bar, obtained by averaging all the data point error bars. Some of the detected sources have colours consistent with those of the absorbed power-law or absorbed bremsstrahlung models, others seem to require combined spectra or fall outside the pattern area. Even if many sources appear to have spectra consistent with that of a typical AGN (squared dots and close black tracks), we cannot rule out that some of the sources may have a different nature. In fact, due to the large error bars for the HR* values, a classification based only on the hardness ratio cannot constrain the nature of the objects in our sample, and allow us to distinguish AGNs, X-ray binaries, CVs and X-ray active stars.

To improve our classification, we adopted the method of Haakonsen & Rutledge (2009), which uses a colour–colour diagram based on the ratio between the 0.2–2.4 keV flux (F_X) and the NIR flux in the J band (F_J) versus the $J - K$ colour. In particular, QSO and Seyfert 1 objects lie in the upper right part having $(J - K) \gtrsim 0.6$ and $F_X/F_J \gtrsim 3 \times 10^{-2}$ (dashed red lines in Fig. 3). Coronally active stars (including pre-main sequence and main-sequence stars, high proper-motion objects and binary systems) lie on the lower left side with $(J - K) \lesssim 1.1$ (dotted black line in Fig. 3) and $F_X/F_J \lesssim 3 \times 10^{-2}$.

As one can see in Tables 1–4, we found many correlations between the detected sources and the 2MASS catalogue. For these sources, we give in Table 9 the 0.2–2.4 keV and NIR J band fluxes, as well as the J and K magnitudes.

To obtain the 0.2–2.4 keV band flux, we used the 0.2–12.0 keV one assuming, in webPIMMS,[9] a power-law model with spectral index Γ and absorption column density N_H inferred with the NASA online tool.[10] Thus, we obtained $\Gamma = 1.7$ and $N_H = 2.77 \times 10^{20}$ cm^{-2} for Draco, $\Gamma = 1.7$ and $N_H = 3.75 \times 10^{20}$ cm^{-2} for Leo I, $\Gamma = 1.7$ and $N_H = 4.65 \times 10^{20}$ cm^{-2} for UMa II and $\Gamma = 1.7$ and $N_H = 2.20 \times 10^{20}$ cm^{-2} for UMi. In Fig. 3, we present the colour–colour diagrams for the sources listed in Table 9.

[8] The reader can also refer to Ramsay & Wu (2006).

[9] WebPIMMS is available at http://heasarc.gsfc.nasa.gov/Tools/w3pimms.html.

[10] This tool is available at http://heasarc.gsfc.nasa.gov/cgi-bin/Tools/w3nh/w3nh.pl.

Table 9. Detected X-ray sources that correlate with the 2MASS catalogue. Following Haakonsen & Rutledge (2009), we try to constrain their nature using the X-ray (in the 0.2–2.4 keV band) and NIR (J and K bands) fluxes (see text and Fig. 3 for details). Recall that the 2MASS data reach the 3σ limiting sensitivities of 17.1 and 15.3 mag in the J and K bands, respectively. A long dash means that the corresponding source was not detected in the relevant band.

Source	F_X ($\times 10^{-14}$ erg s^{-1} cm^{-2})	F_J ($\times 10^{-13}$ erg s^{-1} cm^{-2})	J	K
		(a) Draco dSph		
1	$\leq$0.48	173.6 ± 3.7	11.17 ± 0.02	10.70 ± 0.02
3	0.21 ± 0.18	2.87 ± 0.19	15.62 ± 0.07	14.61 ± 0.08
10	0.28 ± 0.12	351.6 ± 5.5	10.40 ± 0.02	10.21 ± 0.02
13	0.33 ± 0.17	9.11 ± 0.69	14.37 ± 0.08	13.14 ± 0.08
14	0.33 ± 0.16	1.52 ± 0.15	16.31 ± 0.10	15.42 ± 0.18
19	0.37 ± 0.34	343.3 ± 8.2	10.43 ± 0.03	10.12 ± 0.02
29	0.45 ± 0.14	8.97 ± 0.26	14.38 ± 0.03	13.46 ± 0.04
38	0.61 ± 0.36	13.29 ± 0.38	13.96 ± 0.03	13.33 ± 0.03
39	0.61 ± 0.44	2.67 ± 0.20	15.70 ± 0.08	14.44 ± 0.10
42	0.68 ± 0.14	5.32 ± 0.24	14.95 ± 0.05	14.12 ± 0.08
55	1.04 ± 0.46	1.12 ± 0.17	16.64 ± 0.16	15.38 ± 0.02
80	5.19 ± 0.86	2.13 ± 0.18	15.94 ± 0.09	14.60 ± 0.09
87	10.70 ± 0.56	2086 ± 37	8.47 ± 0.02	7.78 ± 0.02
88	28.9 ± 2.3	4.14 ± 0.24	15.22 ± 0.06	13.86 ± 0.07
89	44.48 ± 0.55	4090 ± 115	7.74 ± 0.03	7.44 ± 0.02
		(b) Leo I dSph		
6	$\leq$0.20	262 ± 5	10.72 ± 0.02	9.96 ± 0.02
96	1.90 ± 0.46	3716 ± 62	7.84 ± 0.02	7.18 ± 0.02
108	3.29 ± 0.27	1117 ± 22	9.15 ± 0.02	8.74 ± 0.02
113	5.70 ± 0.45	0.71 ± 0.15	17.14 ± 0.21	15.16 ± 0.15
		(c) UMa II dSph		
1	0.27 ± 0.19	4.94 ± 0.23	15.03 ± 0.05	14.02 ± 0.06
7	0.40 ± 0.15	31.54 ± 0.78	13.02 ± 0.03	12.31 ± 0.03
8	0.47 ± 0.20	8.36 ± 0.27	14.46 ± 0.04	13.51 ± 0.04
13	0.64 ± 0.30	2.70 ± 0.13	15.69 ± 0.09	14.15 ± 0.08
21	0.92 ± 0.49	1.66 ± 0.16	16.22 ± 0.10	15.25 ± 0.17
26	1.23 ± 0.59	0.83 ± 0.12	16.96 ± 0.15	–
27	1.24 ± 0.14	1973 ± 42	8.53 ± 0.02	8.03 ± 0.02
44	3.92 ± 0.77	49.2 ± 1.2	12.54 ± 0.03	12.13 ± 0.02
48	22.1 ± 1.3	2.14 ± 0.20	15.94 ± 0.10	14.62 ± 0.10
49	63.7 ± 4.8	2.67 ± 0.23	15.70 ± 0.09	14.36 ± 0.09
		(d) UMi dSph		
1	0.23 ± 0.14	1.75 ± 0.15	16.16 ± 0.09	15.11 ± 0.17
13	0.52 ± 0.36	12.26 ± 0.30	14.04 ± 0.03	13.37 ± 0.04
47	2.4 ± 1.2	37.47 ± 0.76	12.83 ± 0.02	12.28 ± 0.02

In particular, Fig. 3(a) shows the 15 sources of Draco dSph with the detected counterparts. Among these, three (55, 80 and 88) clearly reside in the AGN part of the diagram. The likely galactic nature of source 55 is also inferred by the correlation with a QSO (see catalogues 223/qsos and 1921/table10). Sources 1, 3, 10, 14, 19, 29, 38, 42, 87 and 89 may be stellar objects. Many (1, 10, 19, 38, 87 and 89) correlate with PPMX sources, so are probably MW sources. Source 38 is also associated with an object in a late-type star catalogue (442/165), while source 29 is realistically a carbon star (C1), as also reported in the Draco stellar catalogue (1921/table9). Source 10 may be either a star (PPMX catalogue) or a background object (437/968). In this case, the diagram can be useful in determining the stellar type. We cannot use the same method for source 13, correlating with both the PPMX (stellar) and 78/675 (quasar–galaxy association) catalogues, because there is no clear identification in the aforementioned regions of the diagram. Finally, source 39 is not catalogued with our diagram although it seems correlated with an AGN candidate (437/968 catalogue).

For Leo I, we find four sources correlating with the 2MASS catalogue. The position of source 113 in Fig. 3(b) denotes its background nature. The sources 96 and 108, recognized as stellar sources, are also associated with two objects in the PPMX catalogue, so they may be foreground stars.

Fig. 3(c) shows five stellar (1, 7, 8, 27 and 44) and three galactic sources (21, 48 and 49) towards UMa II dSph. We correctly obtain a correlation of source 27 with a source in the PPMX catalogue. In the same catalogue, we find a source correlating with source 44 that has an association with an AGN candidate (437/968 catalogue) so the diagram is useful in fixing the possible stellar nature of the source.

In Fig. 3(d), we present the analysis for UMi dSph. The relevant sources (1, 13 and 47) seem to have characteristics similar to

Table 10. Our source classification criteria. Here LX stands for local X-ray source.

Source type	Criteria
fg star	Classified as star in SIMBAD, $\log(f_X/f_{opt}) < -1.0$, $HR_2 < 0.3$ and $HR_3 < -0.4$ or not defined
SNR	Classified as a supernova remnant (SNR) in SIMBAD, $HR_1 > 0.1$, $HR_2 < -0.4$ and not a fg star
AGN	Classified as AGN, Sy1 or QSO in SIMBAD, not classified as SNR from HR_2
GAL	Classified as G in SIMBAD, optical id with galaxy and $HR_2 < 0.0$
SSS	$HR_1 < -0.2$, $HR_2 - EHR_2 < -0.99$ or HR_2 not defined, HR_3 and HR_4 not defined
Hard	$HR_2 - EHR_2 > -0.2$ or only HR_3 and HR_4 defined and no other classification
LX	Not a fg star, classified as a star in SIMBAD, red shift compatible with dSph

X-ray active stars and binary sources. In particular, source 13 correlates with a radio/X-ray source (V/134 catalogue) with a red (blue) magnitude of 17.0 (20.2) while source 47, correlating also with the PPMX catalogue, is probably a foreground star.

We also used the SIMBAD database to search for correlations between our X-ray sources and available catalogues, getting more information (e.g., magnitude, red shift and source interpretation), which is used later.

Moreover, we follow the method of Pietsch et al. (2004), also used by Bartlett et al. (2012) to classify high-energy sources in Phoenix dSph. These authors statistically evaluated the nature of the sources by considering criteria based on HR values defined as $HR_i = (B_{i+1} - B_i)/(B_{i+1} + B_i)$, with the count rates B_i of the bands given in Section 3. We derive our own criteria, summarized in Table 10, using the criteria fixed by Bartlett et al. (2012) and requesting the relevant classification in SIMBAD (for results of our classification, see Fig. 4 and Table 11). The sources are labelled as identified (i), classified (cl) or candidate (ca) if they fulfil all, the majority or only a few criteria, respectively.

Furthermore, in the last column of Tables 5–8, we report the source classification (HR class) based on these criteria. Here, FG (fg/f) indicates the identified (classified/candidate) foreground stars, snr the classified supernova remnants, A the identified AGNs, G (g) the identified (classified) galaxies, sss the classified super soft sources, h the classified hard sources and Loc (loc/l) the identified (classified/candidate) local X-ray sources.

As the reader can see, the obtained results give a wider X-ray source classification and show good agreement with the previous inferences.

4.2 Background sources

As suggested in the previous discussion, some of the detected sources may be AGNs or background galaxies. We estimate the expected number of background sources towards our targets through the $\log N$–$\log S$ diagram (Hasinger et al. 2005). Starting from the minimum absorbed fluxes (in the 0.2–12.0 keV energy band) and assuming Γ and N_H values as in the previous section, we estimated, via webPIMMS v3.9, the unabsorbed fluxes in the 0.5–2.0 keV energy band to be

$$F^{\rm Unabs}_{0.5-2.0} = 1.67 \times 10^{-15}\ {\rm erg\ s^{-1}\ cm^{-2}}\ \text{for Draco},$$
$$F^{\rm Unabs}_{0.5-2.0} = 4.73 \times 10^{-16}\ {\rm erg\ s^{-1}\ cm^{-2}}\ \text{for Leo I},$$
$$F^{\rm Unabs}_{0.5-2.0} = 2.15 \times 10^{-15}\ {\rm erg\ s^{-1}\ cm^{-2}}\ \text{for UMa II},$$
$$F^{\rm Unabs}_{0.5-2.0} = 1.80 \times 10^{-15}\ {\rm erg\ s^{-1}\ cm^{-2}}\ \text{for UMi}.$$

Using these values as input parameters in the Hasinger relation, we find the expected number of background AGNs as a function of the angular distance from the galaxy centre. To compare the theoretically estimated source number with the observed one, we divided each dSph field of view into five rings and performed a comparison for them. As can be seen in Table 12, the number of X-ray sources in each annulus is generally consistent with the expected one, although this is not the case for the external annuli since $\log N$–$\log S$ does not account for border effects.

Nevertheless, we cannot rule out that some sources actually belong to MW or to the dSphs. This claim is supported by the presence of X-ray sources in the bottom-left region of the panels in Fig. 3 and the correlations with variable star catalogues and the analysis summarized in the following section as well.

4.3 Possible local stars

Next we investigate the local nature of some of the detected high-energy sources.

Draco sources 3, 14 and 42, recognized as stellar objects in Fig. 3(a), are not associated with any of the sources in the PPMX catalogue and so it cannot be excluded that they are local high-energy stellar systems. Source 30 has a 'carbon like star counterpart' at a distance of 0.38 arcsec, as reported by the 1921/table9 catalogue, which has many kinds of stars belonging to Draco. Sources 60, 64 and 77 correlate with late-type stars in Draco but sources 64 and 77 have closer counterparts in two background object catalogues as well. Finally, source 84 is associated with a Draco variable star (within 1 arcsec) of the 127/861 catalogue but also to a QSO at a distance of 0.52 arcsec (0.55 arcsec) in the 1921/table10 (1223/qsos) catalogue. Its local nature is not so clear and we must conclude that source 84 is likely linked to a background source, owing to the smaller distance from this kind of counterpart. The background nature of the last three sources is confirmed by the SIMBAD database. In the same data collection, we find clues for the stellar nature of X-ray sources towards/in Draco dSph.

As regards Leo I dSph, we find 20 correlations between our catalogue and 1475/table2, a NIR catalogue of Leo I stars. One of these sources (source 103) also correlates with a QSO candidate (within ∼2.27 arcsec), so we infer a possible background nature for it. Source 6 seems to have a stellar nature (as already seen in Section 4.1) and no association with PPMX sources, therefore we argue that it belongs to the Leo I galaxy.

For UMa II, sources 1, 7 and 8 may belong to this dSph because of their stellar nature (see Section 4.1) and lack of association with any PPMX object. Furthermore, sources 7 and 8 correlate with objects in the II/313 catalogue, a list of non-variable sources. According to the stellarity index, a star/galaxy discriminator defined by Ofek et al. (2012), these two sources seem not to have an extended profile and could be UMa II stars, lacking foreground hints.

Regarding UMi, sources 1 and 13 are probably stars that belong to UMi because they are recognized as likely stellar objects in Fig. 3(d) but do not show any correlations with the PPMX catalogue.

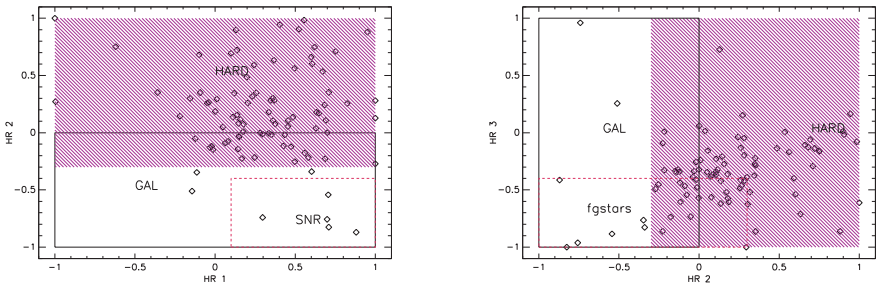

(a) Draco dSph HRs

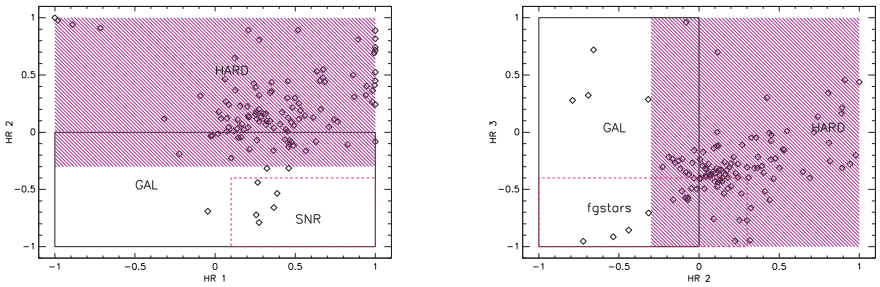

(b) Leo I dSph HRs

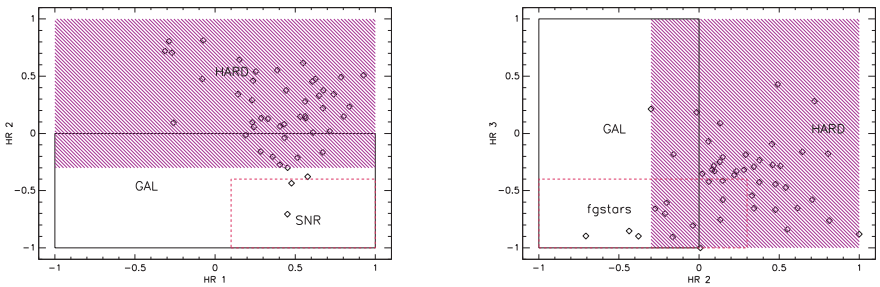

(c) UMa II dSph HRs

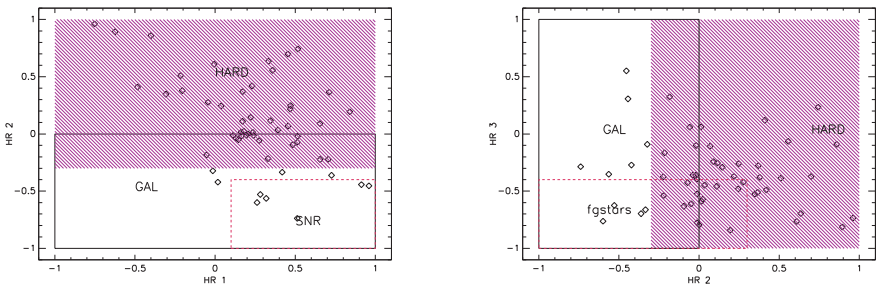

(d) UMi dSph HRs

Figure 4. HR colour–colour diagrams for our X-ray sources (see text for details).

We also perform a more restrictive source analysis, using the method from Pietsch et al. (2004) and Bartlett et al. (2012) and considering as local sources only those identified or classified as such. Therefore, for Draco dSph we have two local sources (the identified 29 and the classified 14), only one (the classified 14) for UMa II and none for Leo I and UMi. A subsequent follow-up (also in other wavelengths) would be useful to probe fully the nature of such objects. In addition, it could have implications for the formation and evolution scenarios of these galactic systems.

Apart from the aforementioned sources, about 30 of them remain at the candidate stage. So, a further study could settle whether they really belong to the dSphs or not.

4.4 Clues for IMBHs

Both the $M_{\rm BH}$–σ and $M_{\rm BH}$–$M_{\rm Bulge}$ relations (e.g., Gebhardt et al. 2000 and Ferrarese & Merrit 2000) suggest searching for compact objects in the IMBH range towards dSphs. For this reason, we look for BHs in their cores, where these X-ray sources are likely located.

The closest source (source 11) to the Draco centre is at a distance of about 51 arcsec. Source 67 (source 3) is 76 arcsec (51 arcsec) from the Leo I (UMa II) centre (see Fig. 5). These distances are well above the source error boxes (1.2, 0.7 and 1.4 arcsec, respectively), so we infer that none of the high-energy sources is located at the centre of these dSphs.

Table 11. Results of dSph source classification using Table 10 (see the text for details).

Type	Draco	Leo I	UMa II	UMi
fg star	5^{i}+7^{cl}+13^{ca}	2^{i}+24^{ca}	11^{ca}	1^{i}+8^{cl}+8^{ca}
SNR	1^{cl}	2^{cl}	0	4^{cl}
AGN	11^{i}	1^{i}	1^{i}	2^{i}
GAL	1^{cl}	1^{i}+1^{cl}	0	0
SSS	0	0	0	0
Hard	28^{cl}	72^{cl}	31^{cl}	10^{cl}
LX	1^{i}+1^{cl}+13^{ca}	1^{ca}	1^{cl}	16^{ca}
Not classified	8	12	5	5

Table 12. Sources expected through the log N–log S diagram and observed in annuli around the galactic centres of our sample. Here, R_{in} and R_{ex} represent the interior and exterior annulus radii, respectively.

Annulus	R_{in} (arcmin)	R_{ex} (arcmin)	# Exp	# Obs
		(a) Draco dSph		
1	0.00	0.76	0.2 ± 0.1	0
2	0.76	3.60	5.6 ± 1.0	7
3	3.60	6.50	13.3 ± 2.4	13
4	6.50	9.00	17.6 ± 3.1	22
5	9.00	16.00	79.4 ± 14.1	46
		(b) Leo I dSph		
1	0.00	0.76	0.6 ± 0.1	0
2	0.76	3.60	13.4 ± 2.2	11
3	3.60	6.50	31.4 ± 5.0	26
4	6.50	9.00	41.7 ± 6.8	25
5	9.00	16.00	188.3 ± 30.7	53
		(c) UMa II dSph		
1	0.00	0.76	0.2 ± 0.1	0
2	0.76	3.60	4.5 ± 0.9	3
3	3.60	6.50	10.9 ± 2.0	13
4	6.50	9.00	14.4 ± 2.6	11
5	9.00	16.00	65.1 ± 11.6	22
		(d) UMi dSph		
1	0.00	0.76	0.3 ± 0.1	1
2	0.76	3.60	6.1 ± 1.8	5
3	3.60	6.50	14.6 ± 4.3	10
4	6.50	9.00	19.2 ± 5.6	12
5	9.00	16.00	86.8 ± 25.4	26

Nevertheless, using the minimum unabsorbed fluxes and the distances reported by NED, we estimated an upper limit for the luminosity (in the 0.2–12.0 keV energy band) of the compact central object (if any), getting about 4.75×10^{33}, 1.21×10^{34} and 1.05×10^{33} erg s^{-1} for Draco, Leo I and UMa II, respectively.

Scaling the previous minimum fluxes to the 0.5–2.0 keV energy band, we obtained, via the log N–log S relation, the expected number of background sources (within 25 arcsec): $0.08^{+0.18}_{-0.03}$, $0.18^{+0.07}_{-0.06}$ and $0.06^{+0.10}_{-0.02}$, respectively. These being well below unity, we infer that if any source exists in such a region, it should be located within the dwarf galaxies.

Despite any clear identification of a central object, we also put an upper limit on the putative central BH mass (M_{BH}) by assuming it accretes through the Bondi–Hoyle spherical model. Bondi & Hoyle (1944) claimed that when a BH moves with velocity v through a gaseous medium, characterized by hydrogen number density n, it accretes at a rate given by

$$\dot{M} \simeq \frac{4\pi (G M_{BH})^2 m_p n}{(v^2 + c_s^2)^{3/2}}, \quad (3)$$

where m_p is the proton mass and c_s the speed of sound in the medium. Then, the subsequent X-ray luminosity $L_X \simeq \epsilon \eta \dot{M} c^2$ can be rewritten as

$$L_X \simeq \epsilon \eta \, 8.8 \times 10^{36} \left(\frac{M_{BH}}{10^3 \, M_\odot}\right)^2 \left(\frac{V}{15 \, km \, s^{-1}}\right)^{-3} \times \left(\frac{n}{0.1 \, cm^{-3}}\right) erg \, s^{-1},$$

with $V = (v^2 + c_s^2)^{1/2}$, while ϵ is the efficiency in converting mass to radiant energy and η the fraction of the Bondi–Hoyle accretion rate on to the BH.

Assuming $v \simeq c_s \simeq 10$ km s^{-1} (consequently $V \simeq 15$ km s^{-1}) and n in the range 10^{-3}–10^{-1} cm^{-3} as typical values for this kind of system, we obtain that the IMBHs (if any) at the centre of these galaxies must have an upper mass limit of $\sim$100 M$_\odot$. Of course, this estimate scales as $(\epsilon\eta)^{-0.5}$. We also searched for radio sources in the NRAO VLA Sky Survey (NVSS) (within 100 arcsec from the dSph centres) with the aim of obtaining a better BH mass estimate. However, no radio sources were found.

4.5 UMi dSph

The possibility that UMi dSph hosts a BH in its centre has been studied quite intensively. For example, Maccarone, Fender & Tzioumis (2005a) found a radio source within a 3σ error box from the galaxy centre and, assuming the existence of an accreting IMBH and a gas density as low as 1/30 to 1/100 of the typical density in globular clusters, these authors realized that a central BH with a mass of a few 10^5 M$_\odot$ would be necessary to explain the observed radio flux. Furthermore, Lora et al. (2009) inferred an upper limit of 2–3 $\times$ 10^4 M$_\odot$ using N-body simulations of the tidal disruption of a long-lived substructure observed on the north-east side of the UMi major axis. It was also claimed that the compact object may not reside in the galactic centre but is offset from it because of gravitational effects.

Nucita et al. (2013b) analysed the X-ray data acquired by the *Chandra* satellite for $\sim$19.8 ks in 2011 (observation id 12754) and found an X-ray source (at J2000 coordinates RA = $15^h09^m14^s.37$ and Dec = $67^\circ12'58.4''$, with associated error $\sim$0.52 arcsec) with an unabsorbed 0.5–7.0 keV flux of $F^{Unabs}_{0.5-7.0\,keV} \simeq 4.9 \times 10^{-15}$ erg s^{-1}. The X-ray source was spatially coincident (within $\sim$1.2 arcsec) with a source (and already identified in the radio band by Maccarone et al. 2005a) with a flux density of 7.1 ± 0.4 mJy at 1.4 GHz. Such a radio source, 150914+671258, was detected by NVSS at J2000 coordinates RA = $15^h09^m14^s.56$ and Dec = $67^\circ12'58.9''$ and the relevant positional error is $\sim$2.1 arcsec as obtained from the sum in quadrature of the uncertainties associated with the two coordinates. Under the assumption that the observed source is an accreting IMBH, Nucita et al. (2013b) used the Fundamental Plane relation to evaluate the BH mass as $\left(2.9^{+33.6}_{-2.7}\right) \times 10^6$ M$_\odot$. As stressed by the same authors, the detection algorithm (WAVDETECT) was run with a significance threshold of 10^{-6} corresponding to the possibility of there being at least one false detection in the CCD where the target is found. Hence, the source was detected by *Chandra* only at $\sim$2.5σ confidence level.

Here, to test the robustness of this result, we analysed the 2005 *XMM*-Newton data and found that, as shown in Fig. 5(d), an X-ray source (source 3) is clearly detected and superimposed on the

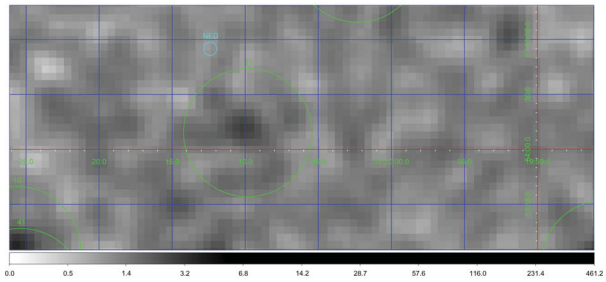

(a) Draco dSph

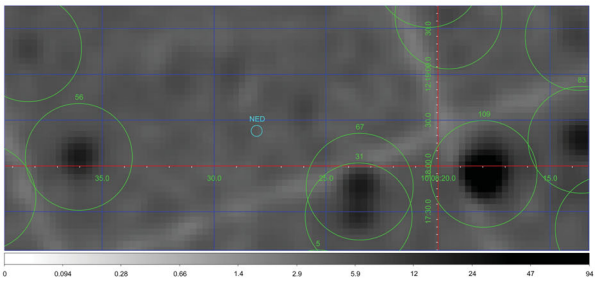

(b) Leo I dSph

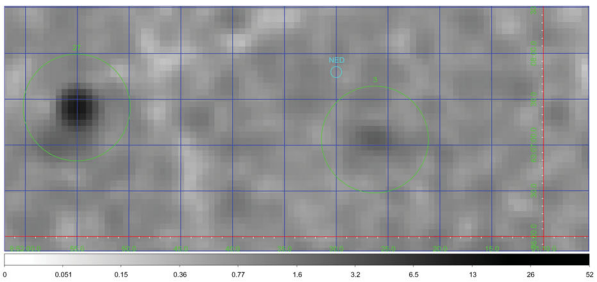

(c) UMa II dSph

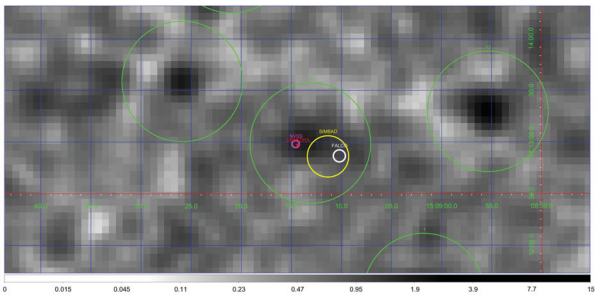

(d) UMi dSph

Figure 5. Zoom view of the four dSph centres. In the last panel, the green, red and magenta circles represent the position of the X-ray source identified at the centre of UMi and its counterparts for *Chandra* and NVSS, respectively. The yellow and white circles show the centres of the galaxy as reported in Falco et al. (1999) and SIMBAD database.

location of the galaxy centre. In particular, source 3 (with J2000 coordinates RA = $15^{\rm h}09^{\rm m}13\overset{\rm s}{.}1$ and Dec = $67^\circ12'59.4''$) has a distance of ∼30 arcsec from the UMi centre (white circle) as reported by Falco et al. (1999),[11] and a galactocentric distance ∼24 arcsec if the SIMBAD database coordinates[12] are considered. In the same figure, we give the position of the X-ray source detected by *Chandra* (1 arcsec, red circle) and the associated NVSS radio counterpart (2 arcsec, magenta circle). Note that the distance between the *XMM*-Newton and *Chandra* sources is ∼7.4 arcsec.

Source 3 is characterized by an absorbed 0.2–12.0 keV flux of $(7.3 \pm 2.9) \times 10^{-15}$ erg s^{-1} cm^{-2}, which corresponds to an unabsorbed flux of $F^{\rm Unabs}_{0.2-12.0\,{\rm keV}} = (7.90 \pm 3.14) \times 10^{-15}$ erg s^{-1} cm^{-2}. The unabsorbed 2–10 keV band flux is $F^{\rm Unabs}_{2-10\,{\rm keV}} = (4.05 \pm 1.61) \times 10^{-15}$ erg s^{-1} cm^{-2}.

Assuming a distance of 73 ± 10 kpc, as reported by NED, we are left with a luminosity $L^{\rm Unabs}_{0.2--12.0\,{\rm keV}} = (4.88 \pm 2.37) \times 10^{33}$ erg s^{-1} and $L^{\rm Unabs}_{2--10\,{\rm keV}} = (2.50 \pm 1.21) \times 10^{33}$ erg s^{-1}.

Following Nucita et al. (2013b) and the references therein, we can get constraints on the possible central BH parameters. In fact, from the correlation between X-ray source 3 and the radio 150914+671258 source (at a distance of ∼3.6 arcsec), we can estimate the BH mass using the Fundamental Plane relation (Merloni, Heinz & Di Matteo 2003; Körding, Falcke & Corbel 2006):

$$\log L_R = \xi_{R_X} \log(L_X) + \xi_{R_M} \log(M_{\rm BH}) + b_R \qquad (4)$$

where the mass and the luminosities are in units of solar masses $M_\odot$ and erg s^{-1}, respectively, $\xi_{R_X} = 0.60^{+0.11}_{-0.11}$, $\xi_{R_M} = 0.78^{+0.11}_{-0.09}$ and $b_R = 7.33^{+4.05}_{-4.07}$. Solving for the BH mass, Merloni et al. (2003) obtained

$$\log(M_{\rm BH}) \simeq 16.3 + \log(D) + 1.28\left[(\log(F_R) - 0.60\log(F_X)\right] \pm 1.06, \qquad (5)$$

where D is the source distance expressed in megaparsecs and the last term is a consequence of the scatter in the Fundamental Plane relation.

From the 1.4 GHz radio flux density of the source 150914+671258, we obtained the 5 GHz one, assuming $F(\nu) \propto \nu^{-\alpha_R}$. So, assuming a flat source spectrum ($\alpha_R \simeq 0$), we get $F(5\,{\rm GHz}) \simeq 7.1$ mJy, consequently a radio flux $F_R = (3.5 \pm 0.2) \times 10^{-16}$ erg cm^{-2} s^{-1} and a radio luminosity of $L_R = (2.19 \pm 0.62) \times 10^{32}$ erg s^{-1}.

Using the previous estimate of the radio (5 GHz) and X-ray (2–10 keV) fluxes in equation (5), we estimate a mass of $\left(2.76^{+32.00}_{-2.54}\right) \times 10^6$ $M_\odot$ for the putative IMBH. The rather large uncertainty is mostly due to the intrinsic scatter of the Fundamental Plane relation. The obtained IMBH mass is consistent with that estimated by Nucita et al. (2013b) when analysing the 2011 *Chandra* data. We also note that this result slightly depends on the index α_R of the radio spectral energy distribution. Changing α_R, $M_{\rm BH}$ scales with the factor $(1.4\,{\rm GHz}/5\,{\rm GHz})^{1.28\alpha_R}$. For example, for $\alpha_R \simeq 0.4$ the BH mass is reduced by ∼50 per cent.

Note also that when scaling the 0.2–12 keV source flux (as detected by *XMM*-Newton) to the range 0.5–7 keV, one gets a flux consistent (within the errors) to that estimated using the 2011 *Chandra* data. The corresponding 0.5–7.0 keV luminosity is $L_X = L_{0.5-7.0\,{\rm keV}} = (3.21 \pm 2.17) \times 10^{33}$ erg s^{-1}. By comparing the bolometric luminosity, calculated as $L_{\rm B} \simeq 16 L_X$ (Ho 2008), with the expected Eddington one $L_{\rm Edd} \simeq 1.3 \times 10^{38} (M_{\rm BH}\,M_\odot)$ erg s^{-1}, one gets $L_{\rm B}/L_{\rm Edd} \simeq 1.43 \times 10^{-10}$. This clearly shows that the UMi putative BH is radiatively inefficient. Indeed, assuming the simplified Bondi

[11] Falco et al. (1999) assigned a positional uncertainty of ∼3.5 arcsec, obtained as a sum in quadrature of the errors (∼2.5 arcsec) associated with RA and Dec, to the UMi galaxy centre.

[12] UMi dSph is located, as reported by SIMBAD (yellow circle), at J2000 coordinates RA = $15^{\rm h}09^{\rm m}11\overset{\rm s}{.}34$ and Dec = $67^\circ12'51.7''$ with a positional uncertainty of ∼12.2 arcsec, due to the sum in quadrature of the RA (∼2 arcsec) and Dec (∼12 arcsec) errors.

accretion scenario, we use equation (4) with $L_X = L^{\rm Unabs}_{0.2-12.0\,{\rm keV}}$ and obtain

$$\epsilon\eta \simeq 7.3 \times 10^{-11} \text{ to } 7.3 \times 10^{-9}, \quad (6)$$

which confirms the expected low IMBH accretion efficiency, previously highlighted.

Finally, we evaluate the expected number of background objects to investigate the possibility that the high-energy emission of source 3 is due to an object behind it. Using the minimum X-ray detected flux towards UMi, correctly scaled to the 0.5–2.0 keV band ($F^{\rm Una}_{0.5--2.0\,{\rm keV}} \simeq 1.80 \times 10^{-15}$ erg s^{-1} cm^{-2}), we get $N \simeq 0.07$ within 25 arcsec from the centre. In spite of the small value of N, the background scenario cannot be definitively ruled out.

5 CONCLUSIONS

In this paper, we re-analysed some deep archival *XMM*-Newton data sets to characterize fully the high-energy point-like source population of four dSph MW companions. The ultimate goal is to classify the X-ray sources identified towards our galaxy sample and pinpoint local (or candidate local) sources.

We performed an accurate study obtaining 89 X-ray sources for Draco, 116 for Leo I, 49 for UMa II and 54 for UMi. Albeit these values are statistically consistent with those of background AGNs, theoretically reached via the $\log N$–$\log S$ relation, we cannot rule out the possibility that some sources belong to the same dSphs. This claim is supported by the colour–colour diagram (based on the ratio between 0.2–2.4 keV X-ray and J band NIR fluxes versus the $J-K$ colour). In this way we find that some X-ray sources, correlating with counterparts in the 2MASS catalogue, have a stellar nature (see Fig. 3 and Section 4.1). Further, we perform a statistical source sorting using only the high-energy data. This leads us to a wider and more complete classification of the X-ray sources in the target field of view. We reveal two high-energy sources belonging to Draco (one of which is a carbon star), one to UMa II and none to Leo I. Although the statistical data we used are poor, finding a few possible local X-ray sources may be a problem that needs to be addressed. In fact, dSph galaxies, as globular clusters, host mainly old star populations but, due to the much lower central stellar density in dSphs, X-ray sources (either LMXBs or CVs) are expected to be primordial objects and not formed by capture encounters. However, these X-ray sources, should already be turned off making it unlikely they are found in dSphs. Finding X-ray sources in dSphs is therefore a puzzling problem and in any case may allow us to test the formation theories of these objects in a contrasting environment with respect to that in globular clusters.

By extrapolating the fundamental $M_{\rm BH}$–$M_{\rm Bulge}$ relation to the dSph realm, one sees that these galaxies are expected to contain IMBHs in their gravitational centres. We thus searched for X-ray sources located within the core radius of the dSphs of our sample. However, for Draco, Leo and UMa we did not identify any high-energy (and radio) sources near the galactic centres. Thus, we can only put upper limits on the mass and luminosity of the putative central IMBHs.

In contrast, it is interesting that the UMi centre hosts an X-ray source, source 3, which correlates in position with a radio object. In the IMBH hypothesis, the Fundamental Plane relation of equation (5) allows us to get an estimate of the mass (a few 10^6 $M_\odot$) of the accreting BH possibly hosted in the galaxy. Recall that the source was detected by *Chandra* but only at the poor $\sim 2.5\sigma$ confidence level, thus leaving the possibility that the *Chandra* source was a mere fake detection.

Our analysis, based on independent *XMM*-Newton data, confirms, however, source 3 as a possible X-ray counterpart of an accreting IMBH.

ACKNOWLEDGEMENTS

We thank M. Guainazzi for stimulating discussions while preparing the manuscript. We also acknowledge the support by the INFN project TaSP. We thank the anonymous referee for the suggestions that greatly improved the paper. One of us (AAN) is grateful to Matteo Nucita for reading the draft.

REFERENCES

Arnaud K. A., 1996, in Jacoby G., Barnes J., eds, Astronomy Society of the Pacific Conference Series Vol. 101, XSPEC: The First Ten Years, in Astronomical Data Analysis Software and Systems V. Astron. Soc. Pac., San Francisco, p. 17
Assmann P., Fellhauer M., Wilkinson M. I., Smith R., 2013a, MNRAS, 432, 274A
Assmann P., Fellhauer M., Wilkinson M. I., Smith R., Blaa M., 2013b, MNRAS, 435, 2391A
Baade W., Swope H. H., 1961, AJ, 66, 300
Bartlett E. S., Coe M. J., Haberl F., McBride V. A., Corbet R. H. D., 2012, MNRAS, 422, 2302
Bellazzini M., Ferraro F. R., Origlia L., Pancino E., Monaco L., Oliva E., 2002, AJ, 124, 3222
Bonanos A. Z., Stanek K. Z., Szentgyorgyi A. H., Sasselov D. D., Bakos G. Á., 2004, AJ, 127, 861
Bondi H., Hoyle F., 1944, MNRAS, 104, 273
Breddels M. A., Helmi A., 2013, A&A, 558, A35
Bukhmastova Yu. L., 2001, Astron. Rep., 45, 581
Carrera R., Aparicio A., Martínez-Delgado D., Alonso-García J., 2002, AJ, 123, 3199C
Casas R. A., Arias V., Peña Ramírez K., Kroupa P., 2012, MNRAS, 424, 1941C
Cavuoti S., Brescia M., D'Abrusco R., Longo G., Paolillo M., 2014, MNRAS, 437, 968
Cioni M. R. L., Habing H. J., 2005, A&A, 442, 165
D'Abrusco R., Longo G., Walton N. A., 2009, MNRAS, 396, 223
Dall'Ora M. et al., 2003, AJ, 126, 197
Dall'Ora M. et al., 2012, ApJ, 752, 42
de la Calle I. et al., eds, 2014, XMM-Newton Proposers Guide and Phase II Remote Proposal System Users Manual, issue 14.0 (ESA: XMM-Newton SOC)
Dehnen W., King A., 2006, MNRAS, 367, 29
Falco E. E. et al., 1999, PASP, 111, 438
Fellhauer M. et al., 2007, MNRAS, 375, 1171
Ferrarese L., Merrit D., 2000, ApJ, 539, L9
Flesch E., 2010, PASA, 27, 283
Gebhardt K. et al., 2000, ApJ, 539, L13
Goranskij V. P., 1982, Astronomicheskii Tsirkulyar, no. 1216
Grillmair C. J. et al., 1998, AJ, 115, 144
Guainazzi M., 2010, XMM-SOC-CAL-TN-0018, XMM-Newton Science Operations Centres http://xmm2.esac.esa.int/docs/documents//CAL-TN-0018.ps.gz
Gullieuszik M., Held E. V., Saviane I., Rizzi L., 2009, A&A, 500, 735
Haakonsen C. B., Rutledge R. E., 2009, ApJS, 184, 138
Harrington R. G., Wilson A. G., 1950, PASP, 62, 365, 118
Harris W. E., 1996, AJ, 112, 1487
Hasinger G., Miyaji T., Schmidt M., 2005, A&A, 441, 417
Held E. V., Gullieuszik M., Rizzi L., Girardi L., Marigo P., Saviane I., 2010, MNRAS, 404, 1475
Ho L. C., 2008, A&A, 46, 475
Ibata R., Irwin M., Lewis G. F., Stolte A., 2001, ApJ, 547, L133
Jardel J. R., Gebhardt K., 2012, ApJ, 746, 89

Kinemuchi K., Smith H. A., Lacluyz A. P., Clark C. L., Harris H. C., Silbermann N., Snyder L. A., 2002, in Aerts C., Bedding T. R., Christensen-Dalsgaard J., eds, Astronomy Society of the Pacific Conference Series Vol. 259, Radial and Nonradial Pulsations as Probes of Stellar Physics, Astron. Soc. Pac., San Francisco, p. 130. Also IAU Colloquium 185
Kinemuchi K., Harris H. C., Smith H. A., Silbermann N. A., Snyder L. A., La Cluyz A. P., Clark C. L., 2008, ApJ, 136, 1921
Kirsch M. G. F. et al., 2004, Proc. SPIE, 5488, 103
Koch A., Wilkinson M. I., Kleyna J. T., Gilmore G. F., Grebel E. K., Mackey A. D., Evans N. W., Wyse R. F. G., 2007, ApJ, 657, 241
Körding E., Falcke H., Corbel S., 2006, A&A, 456, 439
Lemons S. M., Reines A. E., Plotkin R. M., Gallo E., Greene J. E., 2015, ApJ, 805, L12
Lora V., Snchez-Salcedo F. J., Raga A. C., Esquivel A., 2009, ApJ, 699, L113
Maccarone T. J., Fender R. P., Tzioumis A. K., 2005a, Astrophys. Space Sci., 300, 239
Maccarone T. J., Kundu A., Zepf S. E., Piro A. L., Bildsten L., 2005b, MNRAS, 364, L61
Magorrian J., Tremaine S., Richstone D., 1998, AJ, 115, 2285
Majewski S. R., Ostheimer J. C., Patterson R. J., Kunkel W. E., Johnston K. V., Geisler D., 2000, AJ, 119, 760
Malyshev D., Neronov A., Eckert D., 2014, Phys. Rev. D, 90, 103506
Martin N. F., de Jong J. T. A., Rix H.-W., 2008, ApJ, 684, 1075
Martínez-Delgado D., Alonso-García J., Aparicio A., Gómez-Flechoso M. A., 2001, ApJ, 549, L63
Mateo M., 1997, in Arnaboldi M., Da Costa G. S., Saha P., eds, Astronomy Society of the Pacific Conference Series Vol. 116, The Nature of Elliptical Galaxies. Astron. Soc. Pac., San Francisco, p. 259
Mateo M., Olszewski E. W., Morrison H. L., 1998, ApJ, 508, L55
McConnachie A. W., 2012, AJ, 144, 4
Menzies J. W., Whitelock P. A., Feast M. W., Matsunaga N., 2010, MNRAS, 406, 86
Merloni A., Heinz S., Di Matteo T., 2003, MNRAS, 345, 1057
Monet D. G., Levine S. E., Canzian B., 2003, AJ, 125, 984
Muñoz R. R., Geha M., Willman B., 2010, AJ, 140, 138
Nemec J. M., 1985, AJ, 90, 204
Nucita A. A., Manni L., De Paolis F., Vetrugno D., Ingrosso G., 2013a, A&A, 550, 18
Nucita A. A., De Paolis F., Manni L., Ingrosso G., 2013b, New Astron., 23, 107
Odenkirchen M. et al., 2001, ApJ, 122, 2538
Ofek E. O. et al., 2012, PASP, 124, 854
Orio M., Gallagher J., Greco C., Held E., Walker N. H., Pavan L., 2010, AIP Conf. Proc., 1314, 337
Pietsch W., Misanovic Z., Haberl D., Ehle M., Trinchieri G., 2004, A&A, 426, 11
Podsiadlowski Ph., Rappaport S., Pfahl E., Han Z., Beer M. E., 2004, in Rasio F. A., Stairs I. H., eds, Astronomy Society of the Pacific Conference Series Vol. 328, Binary Radio Pulsars. Astron. Soc. Pac., San Francisco, p. 327
Ramsay G., Wu K., 2006, A&A, 459, 777
Rave H. A., Zhao C., Newberg H. J., Yanny B., Schneider D. P., Brinkman J., Lamb D. Q., 2003, ApJS, 145, 245
Reines A. E., Greene J. E., Geha M., 2013, ApJ, 775, 116
Richards G. T. et al., 2009, ApJS, 180, 67
Roeser S., Schilbach E., Schwan H., Kharchenko N. V., Piskunov A. E., Scholz R. D., 2008, A&A, 488, 401
Roeser S., Demleitner M., Schilbach E., 2010, AJ, 139, 2440
Silk J., Wyse R. F. G., Shields G. A., 1987, ApJ, 322, 59
Skrutskie M. F. et al., 2006, AJ, 131, 1163
Smecker-Hane T. A., Marsteller B., Cole A., Bullock J., Gallagher J. S., 2009, Bull. American Astron. Soc., 41, 235
Smith R., Fellhauer M., Candlish G. N., Wojtak R., Farias J. P., Blaña M., 2013, MNRAS, 433, 2529
Stetson P. B., Hesser J. E., Smecker-Hane T. A., 1998, PASP, 110, 533
Walker M. G., Mateo M., Olszewski E. W., 2007, ApJ, 667, L53
Watson M. G. et al., 2009, A&A, 493, 339
Wilson A. G., 1955, PASP, 67, 394, 27
Yang Y., Hammer F., Fouquet S., Flores H., Puech M., Pawlowski M. S., Kroupa P., 2014, MNRAS, 442, 2419
Zinn R., Searle L., 1976, ApJ, 209, 734
Zucker D. B. et al., 2006, ApJ, 650, L41

SUPPORTING INFORMATION

Additional Supporting Information may be found in the online version of this article:

Table 1. X-ray sources towards the Draco dSph as detected by the *XMM*-Newton satellite.
Table 2. X-ray sources towards the Leo I dSph as detected by the *XMM*-Newton satellite.
Table 3. X-ray sources towards the UMa II dSph as detected by the *XMM*-Newton satellite.
Table 4. X-ray sources towards the UMi dSph as detected by the *XMM*-Newton satellite.
Table 5. Correlation of the X-ray sources towards the Draco dSph.
Table 6. Correlation of the X-ray sources towards the Leo I dSph.
Table 7. Correlation of the X-ray sources towards the UMa II dSph.
Table 8. Correlation of the X-ray sources towards the UMi dSph.
(http://mnras.oxfordjournals.org/lookup/suppl/doi:10.1093/mnras/stv1009/-/DC1).

Please note: Oxford University Press are not responsible for the content or functionality of any supporting materials supplied by the authors. Any queries (other than missing material) should be directed to the corresponding author for the paper.

This paper has been typeset from a TEX/LATEX file prepared by the author.